Journal of Manufacturing Processes 30 (2017) 406–417

Contents lists available at ScienceDirect

Journal of Manufacturing Processes

journal homepage: www.elsevier.com/locate/manpro

Research Paper

Mechanistic models and experimental analysis for the torque in FSW considering the tool geometry and the process velocities

Karen J. Quintana[a,b], Jose Luis L. Silveira[b,*]

[a] Department of Mechanical Engineering, COPPE, Universidade Federal do Rio de Janeiro, Brazil
[b] Cidade Universitária, Ilha do Fundão, Centro de Tecnologia, Bloco G, Sala 204 P.O. Box 68503, CEP 21941-972, Rio de Janeiro, RJ, Brazil

ARTICLE INFO

Article history:
Received 12 June 2017
Received in revised form
27 September 2017
Accepted 29 September 2017

Keywords:
Friction stir welding
Mechanistic torque models
FSW experiments

ABSTRACT

Friction Stir Welding (FSW) offers great advantages over conventional welding due to the absence of melting and a small energy requirement. Consequently, the quality of the welded join is better. Torque is a fundamental process quantity in FSW because it is related to weld quality, process control, and mechanical properties of the weld. However, models and experimental studies to determine the effect of each tool part on the torque during the plunging and welding phases have received little attention. In this paper, the influence of the pin and shoulder on the torque is separately considered and three models are developed to describe the torque as a function of the tool geometry and the rotational, plunging and welding speeds. The first model considers only the influence of toolís pin, the second model considers only toolís shoulder and the third model considers the complete tool. The torque was measured during FSW experiments for different combinations of the main welding parameters. The experimental results were used to estimate the model parameters via inverse problem. The results showed a good agreement between the experimental data and the models.

1. Introduction

Friction stir welding is a solid-state welding technique mainly developed to weld materials with poor weldability such as aluminum, magnesium, copper, and other light alloys [1–4]. In the FSW the material does not reach the melting temperature; therefore, the welds obtained have good quality and good properties, the welding process is more healthy, environmentally friendly, and is simple and cost-efficient [5–7]. Torque is an important quantity in FSW process and is closely related to the temperature in the stir zone, material state, weld quality, and together with the axial force [8] are fundamental to the process control and tool design [9–14]. Yan et al. [10], Upadhyay and Reynolds [15] observed a strong relation between torque and temperature through the local stress. Higher temperatures produce a lower local stress in the material and, consequently, the torque is lower. Additionally, the knowledge of the torque behavior is useful to the proper selection of the equipment to carry out the FSW process and to the process control. Su et al. [16] and Mehta et al. [17] measured the torque using the motor electrical signal of the FSW machine. Some authors [11,18–20] have computed the power in the FSW process as the torque multiplied by the rotational speed. Kumar et al. [14] and Cui et al. [19] observed that the torque behavior as a function of time allows the detection of the different phases in the FSW process.

Considering the importance of the torque in the FSW, several authors have performed experimental studies of the torque during the FSW process for a better comprehension of torque behavior and to determine the influence of the main process variables on this quantity. Table 1 shows the main contributions of experimental studies on torque reported in the literature.

Torque is mainly influenced by the welding and rotational speeds, tool geometry, plunging depth and material properties. Some experimental studies [9,10,15,19,20–22] showed that the torque decreases with higher rotational speeds and conversely increases with higher welding speeds. Additionally, the authors showed that the torque is more influenced by the rotational than the welding speed. Quintana and Silveira [22] founded experimentally that although the influence of the welding speed on the torque is considerably smaller than the influence of the rotational speed, the torque behavior is influenced by the interaction of both speeds. Moreover, the authors adjusted an experimental torque model via inverse problem method, and using experimental data from literature founded a strong influence of the tool geometry on the torque behavior. Khandkar et al. [11] and Schmidt et al. [18] determined

* Corresponding author at: Cidade Universitária, Ilha do Fundão, Centro de Tecnologia, Bloco G, Sala 204 P.O. Box 68503, CEP 21941-972, Rio de Janeiro, RJ, Brazil.
E-mail addresses: kjq.cuellar@mecanica.coppe.ufrj.br (K.J. Quintana), jluis@mecanica.ufrj.br, jluis@mecanica.coppe.ufrj.br (J.L.L. Silveira).

https://doi.org/10.1016/j.jmapro.2017.09.031
1526-6125/

Table 1
Main experimental torque studies in FSW.

Year	Authors	Sheet material	Tool material	Welding speed (mm/min)	Rotational speed (rpm)
2005	Yan et al. [10]	AA2524-T351	–	126.6	150 – 800
2007	Long et al. [9]	AA5083-O AA2219-T87 AA7050-T751	H13	102	Variable, with increment rate: 1.4 rpm/mm
2007	Pew et al. [20]	AA7075-T7351 AA5083-H32 AA2024-T3	H13	127–279 127 – 279 51 – 152	200 – 800 200 – 700 175 – 350
2010	Upadhyay et al. [15]	AA7050-T7451	Shoulder: H13 Pin: MP-159	102 – 612	150 – 1000
2010	Cui et al. [19]	AA356	H13	28 – 450	63 – 1400
2012	Leitao et al. [21]	AA5083-H111 AA6082-T6	–	50 – 700	300 – 1100
2012	Kumar et al. [14]	AA5083-H112	H13	80, 120	420, 500
2013	Su et al. [16]	AA2024	–	40 – 120	600 – 1000
2017	Quintana and Silveira [22]	AA5052-H34	H13	100 – 300	600 – 1500

Table 2
Main torque models for FSW reported in the literature.

Year	Author	Sheet material	Tool material	Model type
2003	Khandkar et al. [11]	AA6061-T651	–	Analytical
2004	Schmidt et al. [18]	AA2024-T3	Steel	Analytical
2007	Pew et al. [20]	AA7075-T7351 AA5083-H32 AA2024-T3	H13	Experimental
2009	Arora et al. [23]	AA2524	–	Numerical
2010	Cui et al. [19]	AA356	H13	Experimental
2014	Zhang et al. [24]	AA6061-T6	–	Numerical

that the torque value involves the tool geometry and the properties of the weld material.

Phenomena such as heat transfer, heat generation rate and material flow in FSW have been widely modeled. However, models to describe the torque behavior are not as frequent and enough to its comprehension. Table 2 presents the most important models reported in the literature that were developed to describe the torque behavior. Khandkar et al. [11] described the torque behavior as a function of the contributions of the interfaces tool-material. The authors used the torque value in a model to predict the temperature distribution in the FSW process. Schmidt et al. [18] considered three types of contact conditions in the tool-material interface to describe the torque: sticking condition, sliding condition when the friction condition is assumed in the interface, and partial sticking/sliding condition. The computed torque value was used to describe the heat input in the FSW. Pew et al. [20] used the statistical software MINITAB to describe the torque behavior for aluminum alloys 7075, 5083, and 2024 based on experimental observations. The authors proposed statistical torque models for each material as a function of tool depth and rotational and welding speeds.

Although several authors had studied the torque as a function of the tool geometry and the rotational and welding speeds, both experimentally and by modeling, these studies are not enough to determine the contribution of each part of the tool and the plunging speed on the torque during the two phases of the FSW process (the plunging and the welding). With the goal of advancing the understanding of fundamental mechanics of the FSW process, in this paper, three mechanistic models to describe the torque behavior as a function of tool geometry, rotational, plunging and welding speeds are developed. In order to evaluate separately the influence of the pin and shoulder of the tool on the torque in the plunging and welding phases, the first model considers only the influence of toolís pin in the plunging phase, the second model considers only toolís shoulder in the plunging phase and the third model considers the complete tool in the plunging and welding phases. Experimental results and the inverse problem method are used to estimate the parameters of the proposed models.

The torque experimental data for the first and second models are obtained at four levels of pin diameter, namely 4.5, 5, 5.5 and 6 mm, and three levels of shoulder diameter, 8, 10 and 12 mm, respectively. Both experimental data were performed at four levels of rotational speed, 600, 900, 1200 and 1500 rpm, additionally, for the first model (only tool pin) three levels of tool plunging speed are considered, namely, 4, 6 and 8 mm/min. For the third model (complete tool), the experimental data are obtained at three levels of welding speed, 100, 200 and 300 mm/min and the same levels of rotational speed used in the others models (600, 900, 1200 and 1500 rpm). For the complete tool, two separate expressions are presented for each phase of the welding procedure, i.e., an initial phase corresponding to the plunging of the tool into the material and the final phase corresponding to the tool displacement to obtain the weld. The comparison between the torque values obtained from the models and the experimental data show a good agreement.

2. Mechanistic torque models description

The methodology implemented to develop the torque models as a function of tool geometry and rotational, welding and plunging speeds is showed in the flowchart of Fig. 1. The expressions for the models are based on the physical phenomena of the FSW process and on the analysis of the experimental torque data. The models parameters are estimated via inverse problem using the experimental torque measurements. If the estimated parameters are constant, the model is calibrated with the experimental results. If not, the parameters are described as a function of the evaluated factors. Finally, the relative differences are evaluated and if necessary the model is adjusted. Each step of these procedures will be presented in detail in next section.

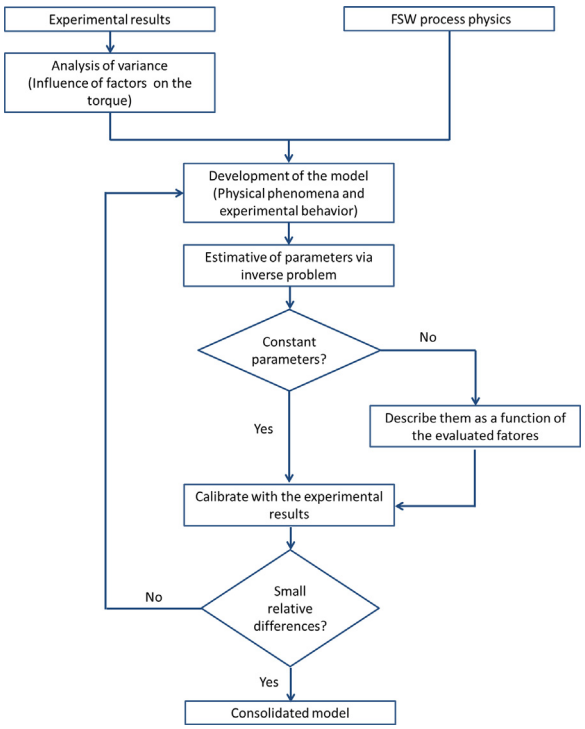

Fig. 1. Methodology to obtain the torque models.

2.1. Torque model for the plunging phase

The torque M_{pp} (Nm) in the plunging phase of the FSW process is defined by Eq. (1) and is given by two separate contributions.

$$M_{pp} = \tau_l G + C v_p \tag{1}$$

The first is the product between the local shear yield stress of the material τ_l (MPa) and a geometric factor $G(m^3)$, and the second is the contribution of the plunging speed v_p (mm/min) multiplied by a parameter C (Nm.min/mm) which is estimated by inverse problem technique.

The local shear yield stress τ_l considers the effect of the heat input in the process by means of the rotational speed due to the strong relation between the rotational speed and the local temperature in the material. Hussein et al. [25] observed experimentally that the rotational speed is the main factor that promotes the growth of temperature and Pew et al. [20] computed the heat input in the FSW process as a function of the rotational and welding speeds and showed that higher rotational speeds increases significantly the heat input of the process. The temperature affects the local yield stress of the material and consequently the torque is also affected.

The geometry factor Gconsiders the contribution of the tool-material interface as given by the following expression:

$$G = \int r dA_s + \int r dA_L + \int r dA_I \tag{2}$$

where A_s, A_L and A_I correspond to the shoulder area, the lateral area of the pin and the inferior area of the pin, respectively, and $r$is the radial distance from the tool center.

2.2. Torque model for the welding phase

The torque M_{wp} (Nm) in the welding phase of the FSW process is described as a function of the torque in the plunging phase M_{pp} and the contribution of the welding speed v_w (mm/min) as presented by the following equation:

$$M_{wp} = M_{pp} + D v_w \tag{3}$$

The D parameter includes the effect of the rotational speed on the torque. Owing to the effect of the temperature during the plunging phase, the material is softened and the local stress is reduced; therefore, the torque value during the welding phase is smaller. The D parameter is described by Eq. (4) as a function of the rotational speed and the parameters D_1 (Nm/(mm/min)) and D_2 (rpm^{-1}) are estimated via inverse problem.

$$D = D_1 e^{-D_2 \omega} \tag{4}$$

For each model, the local shear yield stress and the geometric factor are modeled according to specific conditions of the evaluated phase; the plunging phase for three types of tool geometry (only tool pin, only tool shoulder and complete tool, composed by shoulder and pin) and the welding phase for a complete tool. For each case, the local shear yield stress is described as a function of the rotational speed according to the experimental torque data obtained in each experimental design. The parameters for the expressions for the local shear yield stress are estimated via inverse problem. On the other hand, the geometric factor considers only the contributions of the interfaces involved in each model. Table 3 summarizes the expressions for the geometric factor considered in each model, where h_p is the pin height, r_p is the pin radius and r_s is the shoulder radius.

Table 3
Geometric factor for each model.

Model	Geometric factor, G
First model (only tool pin)	$G = \int_0^{h_p}\int_0^{2\pi} r\left(rd\theta dl\right) + \int_0^{r_p}\int_0^{2\pi} r\left(rd\theta dr\right)$
Second model (only tool shoulder)	$G = \int_0^{r_s}\int_0^{2\pi} r\left(rd\theta dr\right)$
Third model (complete tool)	$G = \int_0^{r_s}\int_0^{2\pi} r\left(rd\theta dr\right) + \int_0^{h_p}\int_0^{2\pi} r\left(rd\theta dl\right) + \int_0^{r_p}\int_0^{2\pi} r\left(rd\theta dr\right)$

3. Torque experimental analysis

3.1. Experimental procedure

A computer numerical control (CNC) machining center adapted to FSW was used to carry out the experiments. A fixture device was designed to guarantee a suitable arrangement of the specimens during the process and, additionally, the Kistler 9272 dynamometer and the multichannel charge amplifier Kistler 5070 was used to measure the torque and for the signal conditioning, respectively. To evaluate separately the influence of the pin and shoulder of the tool on the torque, three experimental designs were accomplished. Aluminum alloy 5052-H34 specimens with 5 mm of thickness were used for all the experiments. The tool material is 1045 steel for the first and the second experimental design and H13 steel, heat treated to an average hardness of 50 HRC for the third experimental design. All experiments were conducted with a tool tilt angle of zero degree.

The first experimental design consists only in the plunging of the tool into the material with a tool composed exclusively of a pin. The

Table 4
Torque value during the welding phase for the third experimental design (complete tool).

Welding speed (mm/min)	Rotational speed (rpm)	Torque welding phase (Nm)	Standard deviation (Nm)
100	600	13.39	0.68
	900	10.30	0.23
	1200	7.75	0.20
	1500	6.26	0.08
200	600	14.65	0.19
	900	9.62	0.39
	1200	7.56	0.33
	1500	6.19	0.11
300	600	14.02	0.92
	900	11.01	0.10
	1200	8.32	0.03
	1500	6.58	0.09

experiments were carried out at four levels of rotational speed: 600, 900, 1200, and 1500 rpm, three levels of plunging speed: 4, 6, and 8 mm/min and four levels of pin diameter d_p: 4.5, 5, 5.5 and 6 mm. A total plunging depth of 4.1 mm was used for all the experiments.

The second experimental design consists only in the plunging of the tool into the material with a tool composed exclusively of a shoulder. The experiments were carried out at four levels of rotational speed: 600, 900, 1200, and 1500 rpm and three levels of shoulder diameter d_s: 8, 10 and 12 mm. A total plunging depth of 0.3 mm was used and a plunging speed of 4 mm/min was kept constant for all the experiments. Owing to the small plunging depth and to facilitate the data acquisition, the total plunging depth (0.3 mm) was kept for 40 s.

The third experimental design comprises all the phases of the FSW process with a complete tool (tool composed by pin and shoulder, d_p: 4 mm and d_s: 10 mm). The welds were carried out at four levels of rotational speed: 600, 900, 1200, and 1500 rpm and three levels of welding speed: 100, 200, and 300 mm/min. A total plunging depth of 4.1 mm was used and a plunging speed of 8 mm/min was kept constant for all the experiments. The dynamometer used in the experiments is able to measure the torque in its center; therefore, two groups of experiments were carried out to obtain the torque values for each phase, the first one for the plunging phase and the second one for the welding phase, during the steady state regime for the torque. Kumar et al. [14] observed experimentally that the torque during the welding phase presents a steady state value.

3.2. Experimental results

3.2.1. Torque behavior during the FSW process

Fig. 2 shows the torque as a function of time for all the experimental designs. In all the cases, the beginning of the plunging phase is in point 1, a stabilization period occurs in point 2 and the end of the experiment, when the tool gets out of the material, is in point 3. In Fig. 2a (first experimental design, only tool pin) the point 3 also represents the total plunging depth of the tool into the material. In Fig. 2b (second experimental design, only tool shoulder) the maximum torque value is observed in the total plunging depth, due to the small penetration of the tool into the material. Fig. 2c (third experimental design, complete tool, plunging phase) at point 4 shows the effect of the shoulder on the torque value when the extruded material due to the penetration of the pin makes contact with the shoulder. The maximum torque value in the plunging phase, when the tool achieves the total plunging depth, is indicated in point 5. The torque during the welding phase presents a steady state value [14] which is presented in Table 4. The torque in the welding phase (for the third experimental design/complete tool) is smaller than the maximum torque value in the plunging phase, due to the softening of the material in the initial phase.

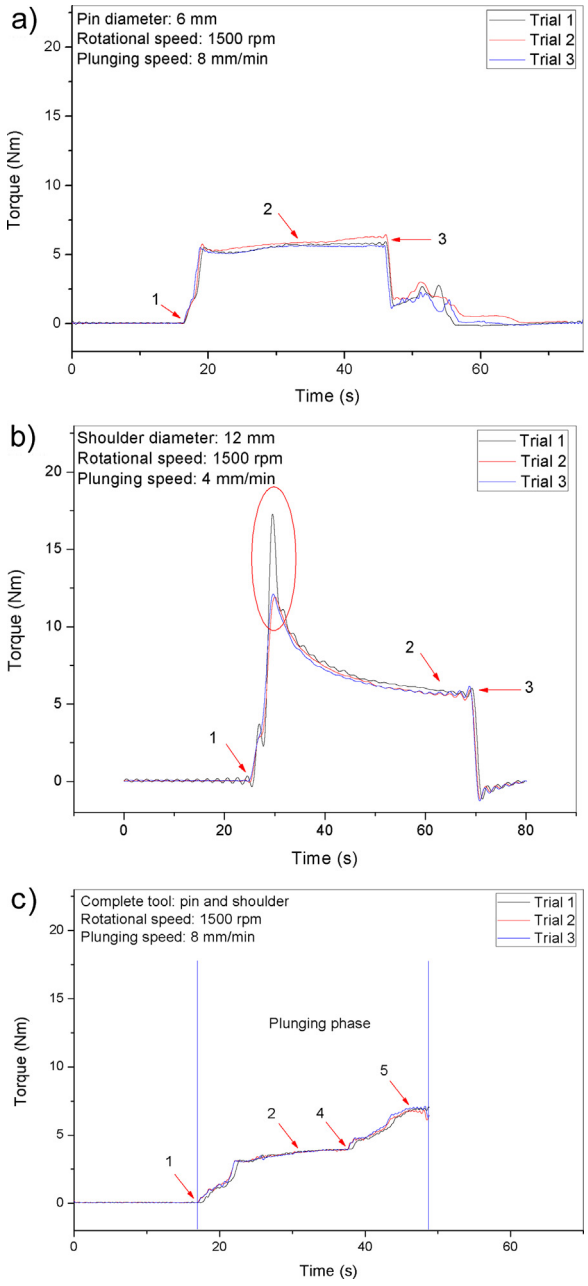

Fig. 2. Torque versus time. a) First experimental design (only tool pin), b) second experimental design (only tool shoulder) and c) third experimental design (complete tool) during the plunging phase.

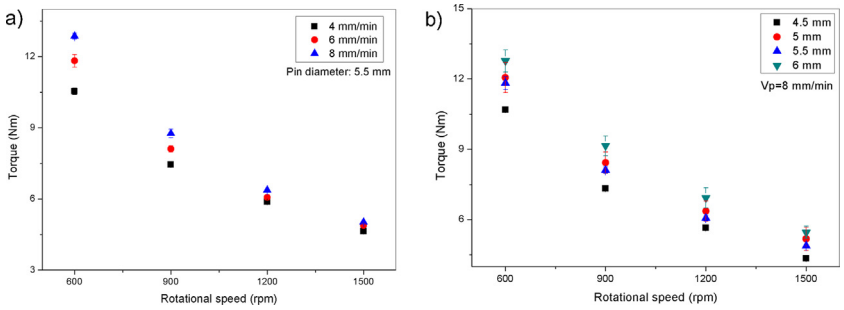

Fig. 3. Experimental data for the torque as a function of the rotational speed for the first experimental design: a) for all plunging speeds and a pin diameter of 5.5 mm and b) for all pin diameters and a plunging speed of 8 mm/min.

Table 5
Analysis of variance (ANOVA) for the torque for the first experimental design.

Source	Sum Sq.	Degree of freedom	Mean Sq.	*F*	*p*-level
ω	943.19	3	314.397	1961.5	0
v_p	33.87	2	16.933	105.64	0
d_p	49.54	3	16.513	103.02	0
$\omega * v_p$	5.68	6	0.947	5.91	0
$\omega * d_p$	3.43	9	0.382	2.38	0.0177
$v_p * d_p$	0.33	6	0.056	0.35	0.9095
$\omega * v_p * d_p$	2.32	18	0.129	0.8	0.6907
Erro	15.39	96	0.16		
Total	1053.76	143			

3.2.2. Torque analysis for the first experimental design

Fig. 3a shows the experimental data for the torque as a function of the rotational speed for all the plunging speeds and for a pin diameter of 5.5 mm. The torque value corresponding to the stabilization value is indicated in Fig. 2a as point 2. It was observed that, the torque is mainly influenced by the rotational speed, owing to the strong relation between the rotational speed and the heat input in the process. Higher rotational speed increases the friction at the tool-material interface and, therefore, increases the local temperature in the material. The torque decreases exponentially with the increase of the rotational speed and increases with higher plunging speed. However, the influence of the plunging speed depends on the rotational speed. For lower rotational speeds, the plunging speed has a greater influence on the torque. As the rotational speed increases, the local temperature increases and the local yield stress decreases; consequently, the torque also decreases and the material is increasingly softened and less affected by other factors, e.g., the plunging speed. Conversely, as plunging speed increases the available time to the heat input is reduced and, consequently, the local yield stress is higher.

Fig. 3b presents the experimental torque data as a function of the rotational speed for all the pin diameters and a plunging speed of 8 mm/min. The torque value increases for higher pin diameters; however, the influence of the pin diameter on the torque is more significant for lower rotational speeds. Increasing the pin diameter increases the tool-material interface and, therefore, the torque value is higher. This behavior was confirmed by the analysis of variance (ANOVA) presented in Table 5, which indicates that for a statistic F of 2.38 and a *p*-level of 0.0177, there exists an interaction between the effects of rotational speed and pin diameter factors on the torque. Additionally, the analysis of variance confirms that, for a statistic F of 5.91 and a *p*-level of 0.000, exists an interaction between the effects of rotational and plunging speeds factors on the torque.

According to the experimental results for the torque presented in Fig. 3, the local shear yield stress of the material τ_l introduced in Eq. (1) is described as an exponential decay function with the rotational speed, for the tool composed only by pin, as shown in the following:

$$\tau_l = Ae^{-B\omega} \tag{5}$$

As it was mentioned in the previous section, the Eq. (5) completes the first model proposed to describe the torque for the plunging phase for a tool composed only by pin. The parameters *A* and *B* in Eq. (5) will be evaluated, in the next section, and if possible they will be estimated via inverse problem, if not, they will be described from the experimental data.

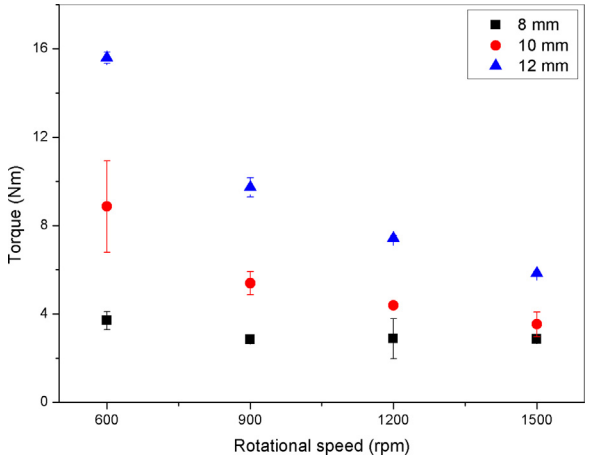

Fig. 4. Experimental data for the torque as a function of the rotational speed, for the second experimental design and all shoulder diameters.

3.2.3. Torque analysis for the second experimental design

Fig. 4 shows the experimental torque data as a function of the rotational speed for all the shoulder diameters. The torque value corresponding to the stabilization value is indicated in Fig. 2b as point 2. The torque value decreases with higher rotational speeds and increases with higher shoulder diameters; however, as the shoulder diameter increases, the influence of the rotational speed on the torque is greater. Taking into account the low plunging depth of the tool in this experimental design, a reduction in the shoulder diameter reduces considerably the contact area and, consequently, the quantity of material affected below the tool is smaller. The results of the torque presented in Fig. 4 shows that for a shoulder diameter of 8 mm, the torque has a little influence on the rotational speed suggesting an interaction of the effects of the evaluated factors on the torque. The analysis of variance (ANOVA) presented in Table 6 confirms that there exists an interaction between the effects of the rotational speed and the shoulder diameter factors on the torque, for a statistic F of 14.84 and a p-level of 0.0.

According to the experimental torque data presented in Fig. 4, the local shear yield stress of the material τ_l presented in the Eq. (1)

Table 6
Analysis of variance (ANOVA) for the torque for the second experimental design.

Source	Sum Sq.	Degree of freedom	Mean Sq.	*F*	*p*-level
ω	146.833	3	48.944	63.8	0
d_s	264.076	2	132.038	172.1	0
$\omega * d_s$	68.307	6	11.384	14.84	0
Erro	18.417	24	0.767		
Total	497.629	35			

Table 7
Analysis of variance (ANOVA) for torque for the third experimental design in the welding phase.

Source	Sum Sq.	Degree of freedom	Mean Sq.	*F*	*p*-level
ω	302.802	3	100.934	465.3	0
v_w	2.166	2	1.083	4.99	0.0154
$\omega * v_w$	4.277	6	0.713	3.29	0.0167
Erro	5.206	24	0.217		
Total	314.451	35			

Table 8
Axial force measurements for all experimental designs. The standard deviation is indicated as SD.

Tool geometry		Plunging speed (mm/min)	Welding speed (mm/min)	Rotational speed (rpm)	Maximum axial force plunging phase (kN)	SD (kN)	Stabilized axial force welding phase (kN)	SD (kN)
Only tool pin d_p (mm)	6	4	–	600	7.14	0.11	–	–
				900	5.08	0.12		
				1200	3.97	0.08		
				1500	3.37	0.02		
		6	–	600	7.64	0.05		
				900	5.37	0.06		
				1200	4.41	0.08		
				1500	3.58	0.02		
		8	–	600	8.22	0.09		
				900	5.82	0.06		
				1200	4.65	0.19		
				1500	4.06	0.11		
Only tool shoulder d_s (mm)	8	4	–	600	3.52	0.12		
				900	3.75	0.05		
				1200	3.53	0.07		
				1500	3.28	0.05		
	10		–	600	5.00	0.14		
				900	5.21	0.10		
				1200	5.18	0.03		
				1500	5.28	0.36		
	12		–	600	5.56	0.14		
				900	6.12	0.19		
				1200	5.98	0.14		
				1500	5.94	0.05		
Complete tool d_p = 4 mm d_s =10 mm		8	100	600	6.59	0.12	3.81	0.19
				900	5.47	0.03	3.44	0.04
				1200	4.88	0.08	3.14	0.08
				1500	4.57	0.05	2.97	0.06
			200	600	6.71	0.18	4.60	0.08
				900	5.38	0.02	3.90	0.11
				1200	4.85	0.06	3.62	0.11
				1500	4.66	0.07	3.48	0.03
			300	600	6.67	0.02	5.00	0.09
				900	5.41	0.06	4.33	0.06
				1200	4.85	0.03	3.88	0.01
				1500	4.39	0.14	3.29	0.17

is described by the following expression, as a logarithmic function of the rotational speed, for the tool composed only by shoulder:

$$\tau_l = A \ln(\omega) + B \quad (6)$$

As it was mentioned in the previous section, the Eq. (6) completes the second model proposed to describe the torque in the plunging phase for a tool composed only by shoulder. The parameters A and B in Eq. (6) will be evaluated and described in the next section.

3.2.4. Torque analysis for the third experimental design

The experimental data for torque in the plunging and welding phase are presented in Fig. 5, as a function of the rotational speed for all the welding speeds. The torque value for the plunging phase corresponding to the stabilization value after the contact between the tool shoulder and the material is indicated in Fig. 2c as point 5. The torque value for the welding phase corresponding to the torque value presented in Table 4. The results show that in both phases (the plunging phase and the welding phase) the torque decreases expo-

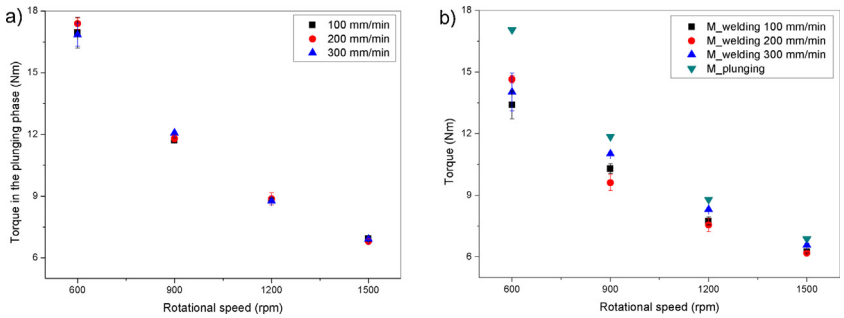

Fig. 5. Experimental data for the torque as a function of the rotational speed for the third experimental design. a) Torque in the plunging phase for all the welding speeds and b) torque in the welding phase for all the welding speeds and the average of the torque value in the plunging phase.

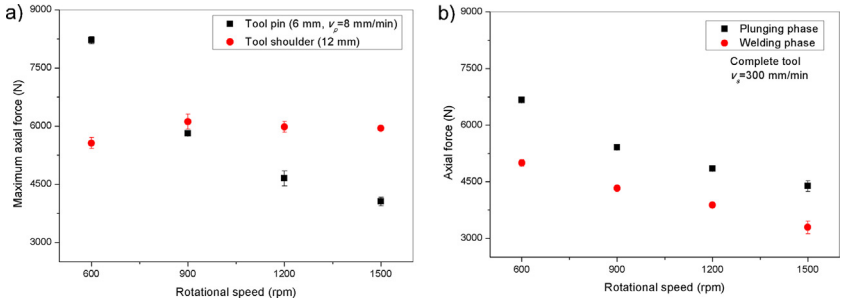

Fig. 6. Axial force as a function of the rotational speed, a) for a tool pin and a tool shoulder during the plunging phase and b) for a complete tool during the plunging and welding phases.

nentially with the increase of the rotational speed. This behavior is related to the heat input proportioned by the rotational speed that softens the material around the tool and decreases the local yield stress and consequently the torque.

According to the experimental results presented in Fig. 5 for the complete tool in the plunging phase, in which the torque presents the same exponential decay with the rotational speed observed in the first experimental design (only tool pin), the local shear yield stress of the material τ_l in the Eq. (1) is also described by the Eq. (5).

On the other hand, the welding speed does not influence the torque during the plunging phase, since the welding speed is only related to the welding phase. Nevertheless, in the welding phase, the torque presents a small increment when the welding speed is increased (Fig. 5). The influence of the welding speed on the torque is significantly smaller than the influence of the rotational speed; however, for higher rotational speeds the influence of the welding speed on the torque is less significant. The increasing of the heat input due to higher rotational speeds decreases the local yield stress of the material and, under these circumstances; the welding speed influence is smaller. The analysis of variance (ANOVA), presented in Table 7, indicates that, for a statistic F of 3.29 and a p-level of 0.0167, the torque in the welding phase is influenced by the interaction of the welding and the rotational speeds factors.

3.2.5. *A summary of the experimental data for axial force*

Taking into account the importance of the axial force in the FSW process, which corresponds to the most critical force acting in the process, the axial force was measured during all the FSW experiments carried out in the present study. Table 8 presents the axial force values for all the experimental designs, during the plunging and welding phases. For the first experimental design (tool pin) only the results for a pin diameter of 6 mm are shown. The axial force values for the other pin diameters presented a similar behavior.

According to the results presented in Table 8, In general, during the plunging phase, the maximum axial force decreases with the increase of the rotational speed and, conversely, the axial force increases with the increase of the plunging speed and the pin/shoulder diameter. As was discussed in the previous sections for the torque, this behavior is related to the heat input into the process and to the increase of the contact area between the tool and the material. For a tool composed only by a shoulder, the maximum force value is not influenced by the rotational speed due to the low plunging depth of the tool that reduces significantly the time to achieve a stabilized maximum value. For the complete tool, the maximum axial force value is presented in the plunging phase; as the welding speed does not have influence on this critical force value. During the welding phase, the axial force remains constant until the end of the FSW experiment. For higher rotational speeds and lower welding speeds, the axial force presented smaller values. For the visualization of the axial force trend, Fig. 6 shows the axial force as a function of the rotational speed for an experiment of each experimental design: for a tool pin of 6 mm of diameter and a tool shoulder of 12 mm of diameter in Fig. 6a and for a complete tool during the plunging and welding phases with a welding speed of 300 mm/min in Fig. 6b.

4. Estimation of parameters

The inverse problem method used to estimate the model parameters followed the procedure described by Quintana and Silveira [22]. The sensitivity coefficients, that represent the sensitivity of the torque in relation to the variation of the model parameters, were founded analytically by differentiating the model expressions with respect to each parameter. The sensitivity coefficients were analyzed to evaluate their absolute values and the linear dependence between them. In order to obtain better estimates, the parameters corresponding to sensitivity coefficients linearly independent were chosen to be estimated simultaneously, i.e., those parameters which are not expressed as a linear combination of each other

Table 9
Estimated values for the parameters of model I (only tool pin) via inverse problem.

Pin diameter (mm)	Plunging speed (mm/min)	Parameter	Estimated value	Standard deviation	Confidence interval (99%)	
4.5	4	A	1.10×10^8	3.47×10^6	1.01×10^8	1.18×10^8
	6		1.24×10^8	3.91×10^6	1.13×10^8	1.30×10^8
	8		1.29×10^8	4.09×10^6	1.19×10^8	1.40×10^8
5	4		1.06×10^8	3.34×10^6	9.70×10^7	1.14×10^8
	6		1.07×10^8	3.40×10^6	9.86×10^7	1.16×10^8
	8		1.12×10^8	3.53×10^6	1.03×10^8	1.21×10^8
5.5	4		7.49×10^7	2.37×10^6	6.88×10^7	8.11×10^7
	6		8.74×10^7	2.77×10^6	8.03×10^7	9.45×10^7
	8		9.95×10^7	3.15×10^6	9.14×10^7	1.08×10^8
6	4		6.71×10^7	2.12×10^6	6.16×10^7	7.25×10^7
	6		7.76×10^7	2.45×10^6	7.12×10^7	8.39×10^7
	8		7.96×10^7	2.52×10^6	7.31×10^7	8.61×10^7
4.5	4	C	-1.90×10^{-2}	4.97×10^{-2}	-1.47×10^{-1}	1.09×10^{-1}
	6		-1.15×10^{-2}	3.73×10^{-2}	-1.00×10^{-1}	8.00×10^{-2}
	8		-6.91×10^{-3}	2.92×10^{-2}	-8.20×10^{-2}	6.82×10^{-2}
5	4		-5.44×10^{-2}	6.10×10^{-2}	-2.11×10^{-1}	1.03×10^{-1}
	6		7.51×10^{-2}	4.10×10^{-2}	-3.05×10^{-2}	1.81×10^{-1}
	8		-9.86×10^{-3}	3.17×10^{-2}	-9.16×10^{-2}	7.18×10^{-2}
5.5	4		5.01×10^{-2}	5.40×10^{-2}	-8.91×10^{-2}	1.89×10^{-1}
	6		-3.75×10^{-2}	4.14×10^{-2}	-1.44×10^{-1}	6.90×10^{-2}
	8		-1.35×10^{-2}	3.49×10^{-2}	-1.03×10^{-1}	7.64×10^{-2}
6	4		1.90×10^{-2}	5.94×10^{-2}	-1.34×10^{-1}	1.72×10^{-1}
	6		5.20×10^{-2}	4.49×10^{-2}	-6.36×10^{-2}	1.68×10^{-1}
	8		6.68×10^{-2}	3.38×10^{-2}	-2.04×10^{-2}	1.54×10^{-1}

and with large absolute values. The parameters that were not estimated via inverse problem due to the linear dependence between their respective sensitivity coefficients and their small absolute values were computed from the experimental data. Reduced sensitivity coefficients were used for ease of comparison between the magnitude of the sensitivity coefficients and the analysis of linear dependence, as defined in Ref. [26], by the product between the sensitivity coefficient and the parameter related to it. The D-optimum design was used to select the optimal maximum rotational speed, and number of measurements for estimating the parameters by means of the variable and fixed frequency analysis, respectively. The Levenberg-Marquardt iterative method was implemented to estimate the parameters using the experimental data as input. Considering that the estimation of the parameters by means of inverse problem require a large number of measurements and the complexity of obtaining experimental data for a wide range of rotational speeds, the trend curve of the experimental data obtained experimentally was used.

For each model, the estimation of parameters was carried out as a function of the rotational speed, for every combination of tool geometry and plunging speed (model I and II), or welding speed (model III). In all the cases, the estimation of parameters was performed for the quantity of rotational speeds and maximum rotational speed suggested by the D-optimal design analysis. The estimated parameters for each combination of factors (tool geometry and plunging or welding speed) were compared, and for the cases that presented different values they were expressed as a function of the evaluated factors for each model.

4.1. Parameters estimation for model I (plunging phase, only tool pin)

The parameters to be estimated for this model are the parameters A, B from Eq. (5) and the parameter C from Eq. (1). Fig. 7a shows the reduced sensitivity coefficients corresponding to these parameters as a function of the rotational speed. The reduced sensitivity coefficient J_A corresponding to the parameter A presents the highest absolute value. The relation between the reduced sensitivity coefficients of the parameters A and B, J_A/J_B, indicates that from 200 rpm there exists a linear dependence between the parameters A and B

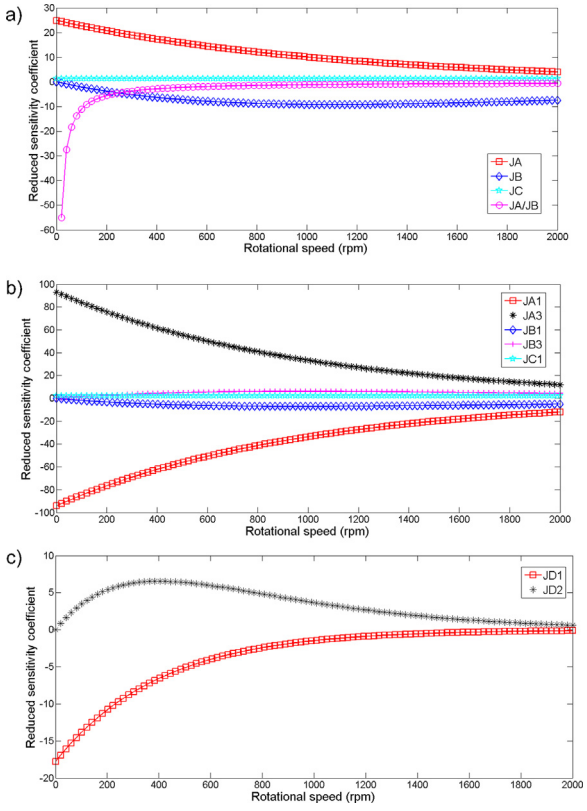

Fig. 7. Reduced sensitivity coefficients as a function of the rotational speed for: a) the first model (only tool pin), b) the third model (complete tool) for the plunging phase and c) the third model for the welding phase.

suggesting that these parameters cannot be estimated simultaneously. Based on the magnitude and the linear independence criteria, the parameters A and C are selected to be estimated via inverse problem. Despite the low magnitude and, therefore, the low sensitivity of the parameter C, this parameter is selected to be estimated as it would provide information about the influence of the plunging speed on the torque. The low magnitude of the reduced sensitiv-

Table 10
Estimated parameters values via inverse problem for model III in the plunging phase (complete tool).

Parameter	Estimated value	Standard deviation	Confidence interval (99%)	
A_3	2.37×10^3	33.23	2.28×10^3	2.24×10^3
B_3	3.95	0.84	1.79	6.1
C_1	9.48×10^2	8.73	-1.3×10^3	3.20×10^3

ity coefficient J_C corresponding to the parameter C is due to the low influence of this parameter on the torque, as observed in the experimental results (Fig. 3a).

The D-optimum design for variable and fixed frequencies analysis identified as optimal values: a rotational speed of approximately 3000 rpm and 2000 measurements, respectively. The initial values for the parameters A and C were obtained from the experimental data. The parameter B was computed by Eq. (7) obtained from the experimental data as a function of the contact area $a_c(\text{mm}^2)$ at the tool-material interface and the plunging speed v_p.

$$B = -(0.481)a_c v_p + (4.176)a_c - 0.0013 \tag{7}$$

The estimated parameters values for each combination of tool geometry and plunging speed are presented in Table 9. Owing to the variation of the estimated values, for each combination of factors, the parameters A and C are described by the following expressions:

$$A = -(6.8 \times 10^9)a_c v_p - (1.487 \times 10^{12})a_c + (4.520 \times 10^6)v_p + 2.048 \times 10^8 \tag{8}$$

$$C = (1.657 \times 10^3)a_c - 0.100 \tag{9}$$

The high standard deviations of the estimated values for the parameter C, presented in Table 9, are related to the low magnitude of the reduced sensitivity coefficient J_C, which indicates that large variations in the parameter C produce small variations in the torque value and, consequently, the estimated values present high standard deviations.

4.2. Parameters estimation for model II (plunging phase, only tool shoulder)

In this model, owing to the small plunging depth (0.3 mm), the influence of the plunging speed is not considered; therefore, the second term of Eq. (1) disappear for a vanishing plunging speed and the parameters to be estimated are only the parameters A and B in Eq. (6). For this reason, in this model, the parameters estimation via inverse problem is unreasonable or unnecessary, as it would estimate the same values for the parameters that would be obtained from the experimental data. Therefore, the parameters A and B are described from the experimental results as a function of the contact area between the tool and the material, as presented in the following expressions:

$$A = -(1.708 \times 10^{11})a_c + 5.782 \times 10^5 \tag{10}$$

$$B = (1.161 \times 10^{12})a_c + 2.438 \times 10^7 \tag{11}$$

4.3. Parameters estimation for model III in the plunging phase (complete tool)

Considering that, for the third experimental design during the plunging phase (experimental data corresponding to the complete tool) the local shear yield stress of the material τ_l in Eq. (1) was described by the same expression used in the model I (Eq. (5)). The parameters A, B and C of the model III, in the plunging phase, are described by the adjustment of the expressions obtained for these parameters in the model I (model for the plunging phase with a tool composed only by pin) Eq. (7)–(9). The coefficients of these equations were analyzed by determining the viability of them to be estimated via inverse problem using the experimental data of the third experimental design as input data. The following expressions corresponding to the Eq. (7)–(9) with the coefficients to be evaluated:

$$A = (A_1 v_p + A_2)e^{(A_3 v_p + A_4)a_c} \tag{12}$$

$$B = B_1 a_c v_p + B_2 a_c + B_3 \tag{13}$$

$$C = C_1 a_c - C_2 \tag{14}$$

Fig. 7b presents the reduced sensitivity coefficients corresponding to the parameters show in Eq. (12)–(14). The sensitivity coefficients corresponding to the parameters A_2, A_4, B_2 and C_2 were not considered due to the small absolute values presented and, therefore, these parameters were taken as the values obtained for the model I. The behavior observed in Fig. 7b indicates that there exists a linear dependence between the sensitivity coefficients J_{A_1} and J_{A_3}, J_{B_1} and J_{B_3}; thence, the parameters A_3, B_3 and C_1 were selected to be estimated simultaneously via inverse problem. According to the D-optimal design, the estimate was carried out for an optimal range of rotational speeds between 0 and 3000 rpm and 2000 measurements. The values estimated for these parameters are presented in Table 10.

4.4. Parameters estimation for model III in the welding phase (complete tool)

The torque during the welding phase for a complete tool is described by Eqs. (3) and (4) where D_1 and D_2 in Eq. (4) are the parameters to be estimated via inverse problem. The reduced sensitivity coefficients of the parameters D_1 and D_2 (presented in Fig. 7c) are linearly independent and, therefore, it is possible to estimate them simultaneously. According to the D-optimal design analysis, the estimate is carried out for an optimal range of maximal rotational speeds between 0 and 1500 rpm and 1000 measurements. The estimated values for each welding speed are presented in Table 11.

5. Models calibration

5.1. Model calibration for model I (plunging phase, only tool pin)

Fig. 8a shows the comparison between the torque experimental data and the torque computed data from the model I, as a function of the rotational speed, for a pin diameter of 4.5 mm and a

Table 11
Estimated parameters values via inverse problem for model III in the welding phase (complete tool), for each welding speed.

Welding speed (mm/min)	Parameter	Estimated value	Standard deviation	Confidence interval (99%)	
100	D_1	−0.0532	0.0112	−0.0822	−0.0244
	D_2	−0.0014	2.44×10^{-4}	−0.0020	−0.0007
200	D_1	−0.0176	0.0061	−0.0334	−0.0019
	D_2	−0.0020	1.33×10^{-4}	−0.0023	−0.0016
300	D_1	−0.0139	0.0039	−0.0240	−0.0038
	D_2	−0.0016	8.58×10^{-5}	−0.0018	−0.0014

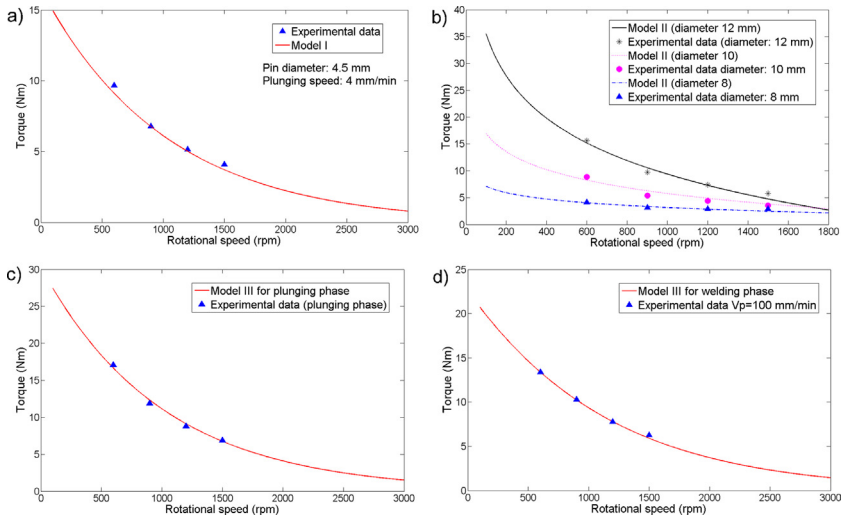

Fig. 8. Comparison between the torque experimental data and the torque computed data as a function of the rotational speed for: a) model I (only tool pin), b) model II (only tool shoulder), c) model III (complete tool) during the plunging phase and d) model III (complete tool) during the welding phase.

Table 12
Relative differences between the torque experimental data and the torque computed by the model I.

Plunging speed (mm/min)	Rotation (rpm)	Relative difference (%)			
		d_p = 4.5 (mm)	d_p = 5 (mm)	d_p = 5.5 (mm)	d_p = 6 (mm)
4	600	2.72	6.04	4.65	1.73
	900	3.26	1.78	11.97	3.45
	1200	1.16	6.58	7.57	3.53
	1500	6.11	0.24	3.29	0.03
6	600	6.03	6.96	0.98	5.96
	900	1.58	0.60	10.68	0.55
	1200	2.34	1.65	11.41	0.36
	1500	6.13	9.84	4.26	3.78
8	600	5.22	4.29	0.35	7.00
	900	1.75	4.64	9.44	4.61
	1200	1.80	0.36	12.59	1.69
	1500	7.51	7.10	7.13	6.48

plunging speed of 4 mm/min. In all the cases, the proposed model presented a good agreement with the experimental torque data. Table 12 presents the relative difference between the torque experimental data and the torque value computed by the model I, for all the torque results obtained in the first experimental design. With the exception of four values, that presented errors of 10.68, 11.41, 11.97 and 12.59%, all the differences are less than 10%. The variation of the error values would be related to the statistical dispersion of the experimental results corresponding to the pin diameter of 5.5 mm.

5.2. Model calibration for model II (plunging phase, only tool shoulder)

Fig. 8b shows the comparison between the torque experimental data and the torque computed data from the model II, as a function of the rotational speed. In all the cases, the torque data obtained from model II presented a good agreement with the experimental torque data. Table 13 presents the relative difference between the torque experimental data and the torque value computed by the model II. With the exception of four values, that presented errors of 11.51, 13.45, 16.44 and 18.51%, the other differences are less than 10%. The high variation of the error values is related to the statistical dispersion of the experimental results, observed in the second experimental design which has the highest statistical dispersion

Table 13
Relative differences between the torque experimental data and the torque computed by the model II.

Rotation (rpm)	Relative difference (%)		
	d_o = 8 (mm)	d_o = 10 (mm)	d_o = 12 (mm)
600	2.72	7.02	2.75
900	6.96	16.44	8.56
1200	0.96	11.51	1.72
1500	13.45	8.08	18.51

of all the experimental designs. Owing to the low plunging depth of the tool, the stabilization of the torque value is more difficult and, consequently, the torque measurements at these conditions presented a high statistical dispersion.

5.3. Model calibration for model III in the plunging and welding phases (complete tool)

Fig. 8c and d shows the torque behavior as a function of the rotational speed obtained experimentally and by the model III in the plunging and welding phases, respectively. For both phases the torque data obtained from model III presented a good agreement with the experimental torque data. Table 14 presents the relative difference between the torque experimental data and the torque value computed by the model III in both phases. In all the cases, the errors values are less than 10%.

6. Conclusions

From the experimental results for the torque and the conditions studied in each experimental design, the following conclusions can be drawn:

- In all the experimental designs, the highest torque value was observed in the plunging phase; therefore, to determine the machine capacity and to design properly the tools for the process, the plunging is the most important phase and the factors that influenced the critical torque value in the FSW are the tool geometry, and the plunging and rotational speeds.
- In this study was observed that the tool pin has a significant influence on the torque as it is the part of the tool that first contacts the material and together with the rotational and plunging speeds provides the heat input to soften the material. Thence, the

Table 14
Relative differences between the torque experimental data and the torque computed by the model III in the plunging and welding phases.

Rotation (rpm)	Relative difference – Plunging phase (%)	Welding speed (mm/min)	Relative difference – Welding phase (%)
600	2.51	100	0.00
900	3.89		0.62
1200	3.09		0.49
1500	1.71		5.56
600		200	9.83
900			5.65
1200			2.94
1500			4.31
600		300	2.74
900			0.88
1200			0.84
1500			5.50

adequate design of the pin can reduce the critical torque in the process and provide a better use of the machine.
- During the plunging phase for a tool composed only by pin and for a complete tool (composed by pin and shoulder) the torque presented an exponential decay with the rotational speed while it presented a slight increase with the increment of the plunging speed. On the other hand, for a tool composed only by shoulder, the torque presented a logarithmic decay with the rotational speed and a slight increase with the increment of the plunging speed. For all the cases, the variance analysis showed that there is an interaction between the effects of rotational and plunging speeds on the torque behavior, suggesting that the influence of these factors on the torque must be analyzed together.
- During the welding phase for a complete tool the torque also presented an exponential decay with the rotational speed and a slight increase with the increase of the welding speed. The variance analysis indicated that there exists an interaction between the effects of the rotational and welding speeds on the torque, suggesting that the influence of these factors on the torque must be analyzed together.

From the mechanistic torque models presented in this paper:

- The models developed for the plunging and welding phases, for all tool types, presented a good agreement with the torque experimental data, considering the contributions of the local shear yield stress, the tool geometry and the rotational, plunging and welding speeds.
- The variation of the estimated/computed values for the parameters of the models for different tool geometries and plunging speeds are in accordance to the analysis of variance. For all the experimental design, an interaction is observed between the effects of the factors on the torque behavior.
- The differences between the torque models and the torque experimental data can be related to the measurement error associated to the equipment, the statistical dispersion of the experimental data, the error related to the estimation of the parameters via inverse problem and the possible errors in the methodology implemented to obtain the models

The models developed for the plunging phase for a tool composed only by pin and for a complete tool might be implemented in the friction stir spot welding while the model proposed for torque in the plunging phase, for a tool composed only by shoulder, might be applied and adapted for the analysis of the torque in friction stir processing.

Acknowledgements

This work was partially supported by CAPES, the Brazilian Federal Agency for Support and Evaluation of Graduate Education; CNPq, the Brazilian National Council for Scientific and Technological Development and FAPERJ, the Foundation for Research Support of the State of Rio de Janeiro, Brazil.

References

[1] Mishra RS, Ma ZY. Friction stir welding and processing. Mater Sci Eng R 2005;50(1–2):1–78, http://dx.doi.org/10.1016/j.mser.2005.07.001.
[2] Mahoney MW, Rhodes CG, Flintoff JG, Spurling RA, Bingel WH. Properties of friction-stir-welded 7075 T651 aluminum. Metall Mater Trans A 1998;29(7):1955–64, http://dx.doi.org/10.1007/s11661-998-0021-5.
[3] Nandan R, Debroy T, Bhadeshia HKDH. Recent advances in friction-stir welding – Process, weldment structure and properties. Prog Mater Sci 2008;53(6):980–1023, http://dx.doi.org/10.1016/j.pmatsci.2008.05.001.
[4] Gerlich A, Su P, North TH. Peak temperatures and microstructures in aluminium and magnesium alloy friction stir spot welds. Sci Technol Weld Join 2005;10(6):647–52, http://dx.doi.org/10.1179/174329305X48383.
[5] Rhodes CG, Mahoney MW, Bingel WH, Spurling RA, Bampton CC. Effects of friction stir welding on microstructure of 7075 aluminum. Scr Mater 1997;36(1):69–115, http://dx.doi.org/10.1016/S1359-6462(96)00344-2.
[6] Rajakumar S, Muralidharan C, Balasubramanian V. Statistical analysis to predict grain size and hardness of the weld nugget of friction stir welded AA6061-T6 aluminium alloy joints. Int J Adv Manuf Technol 2011;57(1):151–65, http://dx.doi.org/10.1007/s00170-011-3279-5.
[7] Qian J, Li J, Sun F, Xiong J, Zhang F, Lina X. An analytical model to optimize rotation speed and travel speed of friction stir welding for defect-free joints. Scr Mater 2013;68(3–4):175–8, http://dx.doi.org/10.1016/j.scriptamat.2012.10.008.
[8] Davis TA, Shin YC, Yao B. Observer-based adaptive robust control of friction stir welding axial force. ASME Trans Mechatr 2011;16(6):10321039, http://dx.doi.org/10.1109/TMECH.2010.2071417.
[9] Long T, Tang W, Reynolds A. Process response parameter relationships in aluminium alloy friction stir welds. Sci Technol Weld Join 2007;12(4):311–7, http://dx.doi.org/10.1179/174329307X197566.
[10] Yan J, Sutton M, Reynolds A. Process–structure–property relationships for nugget and heat affected zone regions of AA2524?T351 friction stir welds. Sci Technol Weld Join 2005;10(6):725–36, http://dx.doi.org/10.1179/174329305X68778.
[11] Khandkar M, Khan J, Reynolds A. Prediction of temperature distribution and thermal history during friction stir welding: input torque based model. Sci Technol Weld Join 2003;8(3):165–74, http://dx.doi.org/10.1179/136217103225010943.
[12] Arora A, Mehta M, De A, DebRoy T. Load bearing capacity of tool pin during friction stir welding. Int J Adv Manuf Technol 2012;61(9-12):911–20, http://dx.doi.org/10.1007/s00170-011-3759-7.
[13] Mehta M, Arora A, De DebRoy T. Tool geometry for friction stir welding-optimum shoulder diameter. Metall Mater Trans A 2011;42(9):2716–22, http://dx.doi.org/10.1007/s11661-011-0672-5.
[14] Kumar R, Singh K, Pandey S. Process forces and heat input as function of process parameters in AA5083 friction stir welds. Trans Nonferrous Met Soc China 2012;22(2):288–98, http://dx.doi.org/10.1016/S1003-6326(11)61173-4.
[15] Upadhyay P, Reynolds AP. Effects of thermal boundary conditions in friction stir welded AA7050-T7 sheets. Mater Sci Eng A 2010;527(6):1537–43, http://dx.doi.org/10.1016/j.msea.2009.10.039.
[16] Su H, Wu CS, Pittner A, Rethmeier M. Simultaneous measurement of tool torque, traverse force and axial force in friction stir welding. J Manuf Proc 2013;15(4):495–500, http://dx.doi.org/10.1016/j.jmapro.2013.09.001.
[17] Mehta M, Chatterjee K, De A. Monitoring torque and traverse force in friction stir welding from input electrical signatures of driving motors. Sci Technol Weld Join 2013;18(3):191–7, http://dx.doi.org/10.1179/1362171812Y.0000000084.

[18] Schmidt H, Hattel J, Wert J. An analytical model for the heat generation in friction stir welding. Modell Simul Mater Sci Eng 2004;12(1):143–57, http://dx.doi.org/10.1088/0965-0393/12/1/013.

[19] Cui S, Chen ZW, Robson JD. A model relating tool torque and its associated power and specific energy to rotation and forward speeds during friction stir welding/processing. Int J Mach Tools Manuf 2010;50(12):1023–30, http://dx.doi.org/10.1016/j.ijmachtools.2010.09.005.

[20] Pew JW, Nelson TW, Sorensen CD. Torque based weld power model for friction stir welding. Sci Technol Weld Join 2007;12(4):341–7, http://dx.doi.org/10.1179/174329307X197601.

[21] Leitao C, Louro R, Rodrigues DM. Using torque sensitivity analysis in accessing friction stir welding/processing conditions. J Mater Process Technol 2012;212(10):2051–7, http://dx.doi.org/10.1016/j.jmatprotec.2012.05.009.

[22] Quintana KJ, Silveira JL. Analysis of torque in friction stir welding of aluminum alloy 5052 by inverse problem method. ASME J Manuf Sci Eng 2017;139(4):041017, http://dx.doi.org/10.1115/1.4035719.

[23] Arora A, Nandan R, Reynolds A, DebRoy P. Torque, power requirement and stir zone geometry in friction stir welding through modeling and experiments. Scr Mater 2009;60(1):13–6, http://dx.doi.org/10.1016/j.scriptamat.2008.08.015.

[24] Zhang Z, Zhang HW. Solid mechanics-Based eulerian model of friction stir welding. Int J Adv Manuf Technol 2014;72(9):1647–53, http://dx.doi.org/10.1007/s00170-014-5789-4.

[25] Hussein SA, Tahir ASM, Izamshah R. Generated forces and heat during the critical stages of friction stir welding and processing. J Mech Sci Technol 2015;29(10):4319–28, http://dx.doi.org/10.1007/s12206-015-0930-3.

[26] Naveira-Cotta CP, Cotta RM, Orlande HRB, Kakac S. Direct and inverse problems solutions. In: Micro-Scale Forced Convection, Microfluidics Based Microsystems (NATO Science for Peace and Security Series A: Chemistry and Biology). Dordrecht, The Netherlands: Springer; 2010. p. 39–59, http://dx.doi.org/10.1007/978-90-481-9029-4_3.